Proceedings of the Sixth International ASME Conference on Nanochannels, Microchannels and Minichannels
ICNMM2008
June 23-25, 2008, Darmstadt, Germany

ICNMM2008-62319

NUMERICAL SIMULATION OF THE PASSAGE OF SMALL LIQUID DROPLETS THROUGH A THIN LIQUID FILM

Minh Do-Quang
Linné Flow Centre, Mechanics Department
Royal Institute of Technology
Stockholm, SE-100 44
Email: minh@mech.kth.se

Göran Stemme
Microsystem Technology, School of Electrical Engineering
Royal Institute of Technology
Stockholm, SE-100 44
Email: stemme@s3.kth.se

Wouter van der Wijngaart
Microsystem Technology, School of Electrical Engineering
Royal Institute of Technology
Stockholm, SE-100 44
Email: wouter@ee.kth.se

Gustav Amberg
Linné Flow Centre, Mechanics Department
Royal Institute of Technology
Stockholm, SE-100 44
Email: gustava@mech.kth.se

ABSTRACT

We simulate numerically a novel method for dispensing, mixing and ejecting of picolitre liquid samples in a single step. The system consists of a free liquid film, suspended in a frame and positioned in front of a droplet dispenser. On impact, a picolitre droplet merges with the film, but due to its momentum, passes through and forms a droplet that separates on the other side and continues its flight. Through this process the liquid in the droplet and that in the film is mixed in a controlled way.

We model the flow using the Navier-Stokes together with the Cahn-Hilliard equations. This system allows us to simulate the motion of a free surface in the presence of surface tension during merging, mixing and ejection of droplets. The influence of dispensing conditions was studied and it was found that the residual velocity of droplets after passage through the thin liquid film matches the measured velocity from the experiment well.

NOMENCLATURE

- α Cahn-Hilliard parameter related to the interface energy.
- β Cahn-Hilliard parameter related to the bulk energy.
- ψ free energy density.
- κ interface mobility.
- η chemical potential.
- ϕ phase field variable.
- ρ density.
- μ dynamic viscosity.
- σ surface tension coefficient.
- ξ mean interface thickness.
- $\mathcal{F}$ free energy.

INTRODUCTION

Dispensing, mixing and ejecting of picolitre volume sample are operations which are of importance in life science applications such as high-throughput drug screening and the generation of microarrays. The generation of ink droplets in the picolitre range forms a core technology in the field of publishing technology. The use of droplet dispensing technology for biotechnical applications is common, however, not uncomplicated due to incompatibility between the ejector operation (heat, electric field, pneumatic pressure etc.) and the liquid properties of biosensitive sample (viscosity, conductivity, saturation pressure etc.). Moreover, the dead volume of a dispenser may require more liquid

sample for priming the device than is physically available or than is economically viable in life science applications.

Geyl et al. [1] introduced the concept of shooting droplets through a freely suspended liquid film, hereby dispensing, mixing and ejecting picolitre liquid samples in a single operation. The experimental work studied the flight of ink droplets, ejected from an inkjet print head, through a free ink film, suspended in a frame and positioned in front of the printhead. The experimentally observed minimum velocity required for the 80 *pL* droplets to fly through the $75 \pm 24\ \mu m$ thick ink film was $6.6\ m\ s^{-1}$. Moreover, a theoretical model was presented, estimating the minimum velocity of a solid sphere passing through a liquid film when taking into account stokes losses.

This work presents a numerical simulation of the passage of liquid droplets through a liquid film in conditions similar to those presented by Geyl *et al.* [1]. The numerical results with different initial speed of droplets and its shapes are taken into account. We observed that the surface energy is partially converted to kinetic energy, and this together with the impact time helps the droplets penetrate the film.

1 Numerical modelling

1.1 Governing equations

In our phase-field model, the order parameter, a phase-field ϕ, is assumed to have a distinct constant value in each phase and to change rapidly but smoothly in the interface region. For example $\phi = 1$ in liquid phase and $\phi = -1$ in gas phase. The free energy of the system can be postulated as

$$\mathcal{F} = \int_\Omega \left(\beta \psi(\phi) - \frac{1}{2} \alpha \nabla^2 \phi \right) d\Omega, \tag{1}$$

where α and β are constants that are related to the surface tension and interface thickness. $\psi(\phi)$ represents the bulk energy of a homogeneous phase, describing the regions far from the interface. In our model, ψ is a double-well potential function that has two minima at $\phi = \pm 1$ corresponding to the two stable phases. A simple example of such a function is,

$$\psi = (\phi + 1)^2 (\phi - 1)^2. \tag{2}$$

The second term in equation (1) describes the interface energy. This term is associated with variations of the phase field ϕ and contributes the free-energy of the interfacial region, which defines the surface tension coefficient [2]

$$\sigma = \alpha \int_{-\infty}^{+\infty} \left(\frac{d\phi_0}{dx} \right)^2 dx = \frac{2\sqrt{2}}{3} \sqrt{\alpha \beta} \tag{3}$$

The fluid flow is described by the Navier-Stokes equations for an incompressible axisymmetric two-phase flow.

$$\frac{\partial \rho \mathbf{u}}{\partial t} + \mathbf{u} \cdot (\nabla \rho \mathbf{u}) = -\nabla p + \nabla \cdot \left[\mu \left(\nabla \mathbf{u} + (\nabla \mathbf{u})^T \right) \right] - \eta \nabla \phi, \tag{4}$$

$$\nabla \cdot \mathbf{u} = 0, \tag{5}$$

$$\frac{\partial \phi}{\partial t} + (\mathbf{u} \cdot \nabla) \phi = \nabla \cdot (\kappa \nabla \eta), \tag{6}$$

where ρ denotes the density, $\mathbf{u}$ the velocity vector, μ the viscosity, and p the pressure. The last term in equation (4) represents the surface tension which is related to the phase-field variables, [3].

The interface is captured by using the Phase-Field method [2, 3], which replaces a sharp interface by a finite thickness, smooth transition region. The phase field ϕ is governed by the convective Cahn-Hilliard equation, equation (6). Here, κ is the constant mobility, η is the chemical potential, defined as,

$$\eta = \beta \frac{\partial \psi}{\partial \phi} - \alpha \nabla^2 \phi. \tag{7}$$

Once the phase field is calculated, the physical properties such as the density and viscosity are calculated as follows,

$$\rho = \rho_l \frac{1+\phi}{2} + \rho_g \frac{1-\phi}{2}, \tag{8}$$

$$\mu = \mu_l \frac{1+\phi}{2} + \mu_g \frac{1-\phi}{2}, \tag{9}$$

where ρ_l, ρ_g and μ_l, μ_g are the densities and viscosities of the liquid and gas phase, respectively.

1.2 Boundary conditions

Neumann conditions are described for the inlet and outlet boundary. The slip boundary condition with zero shear stress for the side and the symmetry edges. Two boundary conditions are needed for the Cahn-Hilliard equation,

$$\mathbf{n} \cdot \nabla \phi = 0, \tag{10}$$

where $\mathbf{n}$ is the unit vector normal to the wall, and,

$$\mathbf{n} \cdot \nabla \eta = 0. \tag{11}$$

1.3 Nondimensionalization

Define the dimensionless variables,

$$x' = \frac{x}{L_c},\ u' = \frac{u}{U_c},\ t' = \frac{t U_c}{L_c},\ p' = \frac{p}{\rho_c U_c^2}, \tag{12}$$

where L_c is the characteristic length taken to be the thickness of the thin film, U_c is the characteristic velocity taken to be the critical velocity in the experiment, $U_c = 6.6\ m\ s^{-1}$. ρ_c is the characteristic density defined as the water density. Dropping the primes, the dimensionless equations are

$$\frac{D(\rho(\phi)\mathbf{u})}{Dt} = -\nabla p + \frac{1}{Re}\nabla\cdot\left[\mu(\phi)\left(\nabla\mathbf{u} + (\nabla\mathbf{u})^T\right)\right] - \frac{1}{Ca\cdot Cn\cdot Re}\eta\nabla\phi, \quad (13)$$

$$\nabla\cdot\mathbf{u} = 0, \quad (14)$$

$$\frac{D\phi}{Dt} = \frac{1}{Pe}\nabla\cdot(\kappa\nabla\eta), \quad (15)$$

$$\eta = \frac{\partial\psi}{\partial\phi} - Cn^2\nabla^2\phi. \quad (16)$$

The dimensionless parameters are the Capillary number Ca, Reynolds number Re and Peclet number Pe and Cahn number Cn,

$$Ca = \frac{\mu_c U_c}{\sigma},\ Re = \frac{\rho_c U_c L_c}{\mu},\ Pe = \frac{U_c L_c}{D}, Cn = \frac{\xi}{L_c}, \quad (17)$$

where μ_c is the characteristic viscosity taken to be the water viscosity, D is the difusivity of liquid vapour in air, $\xi = \sqrt{\alpha/\beta}$ is the interface thickness.

2 Numerical treatment

The numerical simulations were carried out using femLego [4], a symbolic tool to solve partial differential equations with adaptive finite element methods. The partial differential equations, boundary condition, initial conditions, and the method of solving each equation are all specified in a Maple worksheet. The Cahn-Hilliard equation is treated as a coupled system for the chemical potential η and the composition ϕ. Both chemical potential and composition equations are discretised in space using piecewise linear functions and discretised in time using an implicit scheme. The coupled linear systems of η and ϕ are solved simultaneously using the unsymmetric multifrontal method (UMFPACK) [5].

To ensure mesh resolution along the vicinity of the interface, an adaptively refined and derefined mesh is used with an ad hoc error criterion function,

$$\varepsilon\int_{\Omega_k}\nabla^2 C \leq \text{tol}. \quad (18)$$

The implementation of the mesh adaptivity can be described as follows. At each mesh refinement step, an element Ω_k is marked for refinement if the element size is still larger than the minimum mesh size allowed, $h > h_{min}$, and it does not meet the error criterion (18). ε is an ad hoc parameter. In case an element meets the error criterion, it is marked for derefinement unless it is an original element. At the next refinement step, elements containing hanging nodes are marked for refinement. The refinement/derefinement stops if and only if no element is marked for refirement/derefinement. More details about this scheme can be found in [2, 6].

The Navier-Stokes equations are solved using a projection method for variable density that was introduced by Guermond and Quartapelle [7]. The Navier-Stokes equations are also discretised in space using piecewise linear functions with the convective term treated as a semi-implicit term which allows a longer time step in the computations. The linear system is solved by the generalized minimal residual method (GMRES).

3 Numerical results and discussion

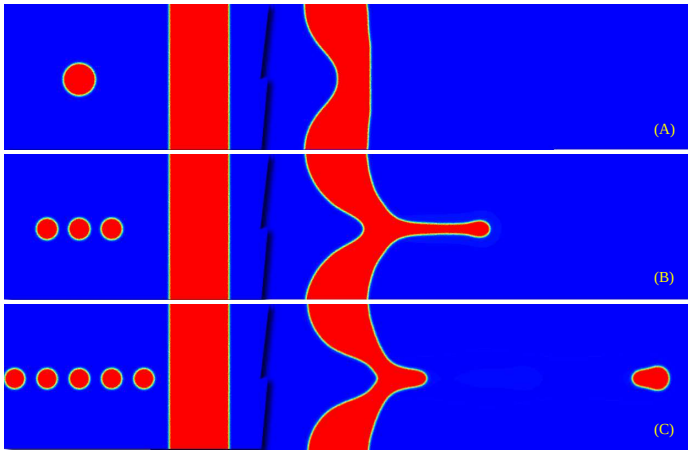

Figure 1. The solution at $t = 0$ (left) and $t = 45.6\ \mu s$ (right) for three different initial conditions.

We begin with the illustration of the behaviour of a droplet, which impacts and passes thought a free hanging liquid thin film, by consideration of a small, non-evaporating droplet having the diameter of $D = 54\ \mu m$. The droplet is moving toward the thin liquid film, $L_c = 92\ \mu m$ thick, at a given initial speed. Both the droplet and the thin film have the same material properties: density of $\rho = 880\ kg\ m^{-3}$, viscosity of $\mu = 0.01\ Ns\ m^{-2}$ and surface tension of $\sigma = 0.032\ N\ m^{-1}$. The computational domain chosen is a cylindrical region, $6L_c$ in radius and $15L_c$ long.

In accordance with the experiment, we tried to shoot a single droplet at a thin liquid film at different speeds from $U_0 = 6\ m\ s^{-1}$ to $13.2\ m\ s^{-1}$. No second droplet created in the other side of

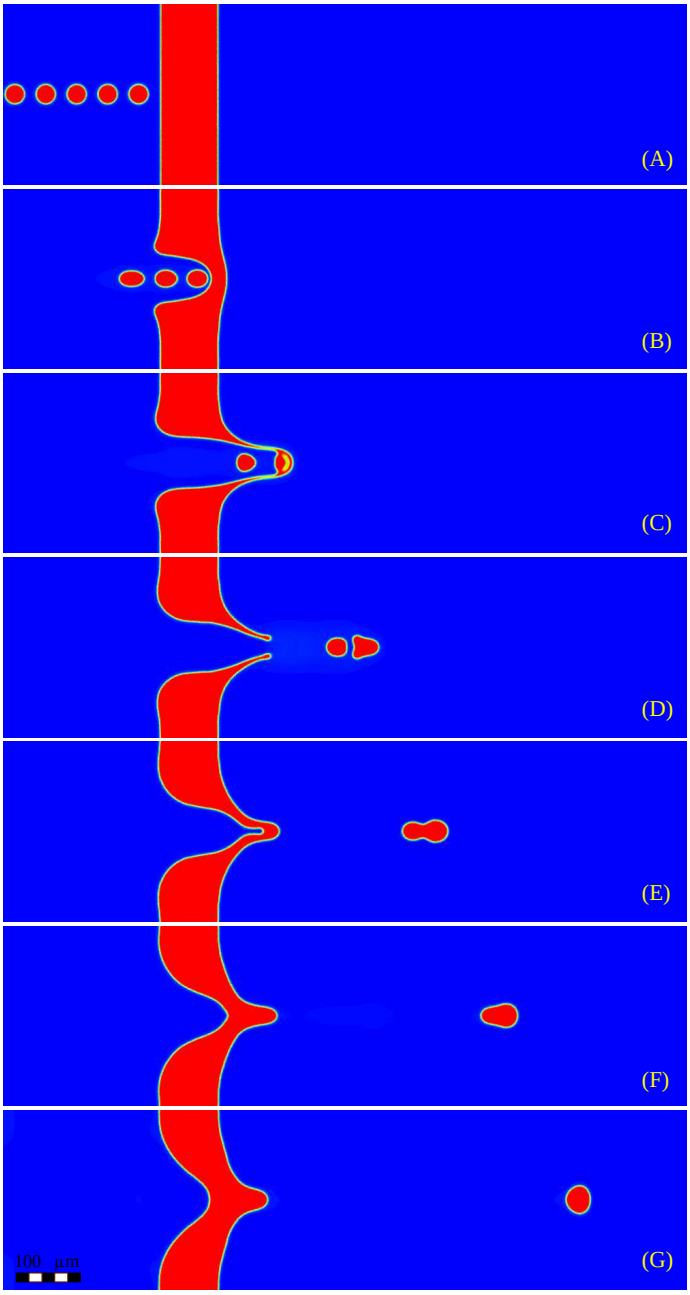

Figure 2. A sequence of pictures of five droplets impact and penetrate the liquid thin film; The initial speed $U_0 = 13.2\ m\ s^{-1}$; (A) $t = 0\ \mu s$, (B) $15.2\ \mu s$, (C) $30.4\ \mu s$, (D) $45.6\ \mu s$, (E) $60.8\ \mu s$, (F) $76\ \mu s$ and (G) $91.2\ \mu s$.

the film had been observed in all tested speeds as seen in the experiment. All droplets trapped in the film. The left panel in Figure 1(A) shows the initial condition for a case with a single droplet at the initial speed $U_0 = 13.2\ m\ s^{-1}$. In the right figure, the solution at $t = 45.6\ \mu s$ obviously shows that the droplet is

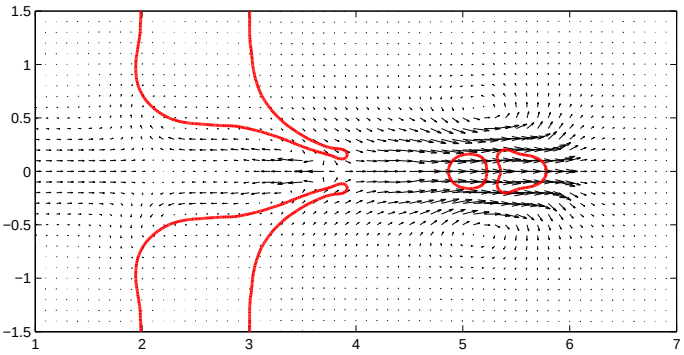

Figure 3. Velocity profile after the droplets passed through the liquid thin film - the solution at $t = 45.6\ \mu s$.

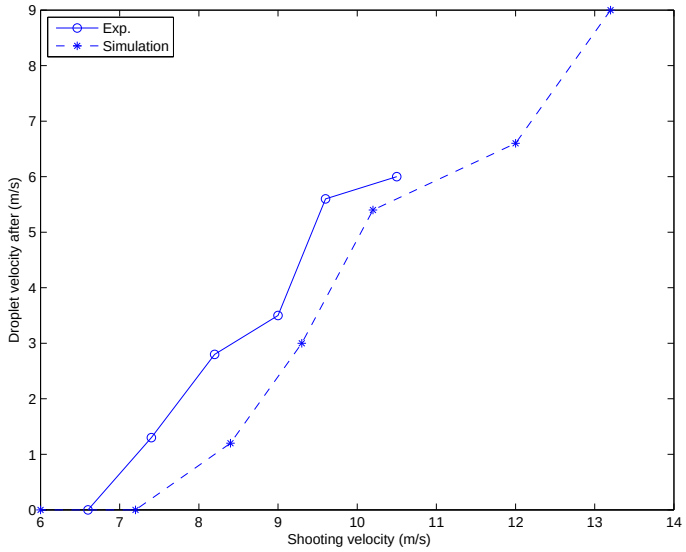

Figure 4. Plot of the residual velocity of droplets after it passed through the thin film vs. the initial velocity

completely trapped in the film, which reverts to the original form due to the surface tension force.

Note that, the droplet with diameter of $D = 54\ \mu m$, is the one we can compute from total volume of a drop ejected at the printhead, $80pl$. However, as observed in the experiments, in fact it did not form a single droplet, but a primary one with a long tail of satellites behind. Therefore, in next simulation, the effect of the different shape of the initialized droplets on the impact between them and the thin liquid film is examined. Figure 1(B) and 1(C) shows the impact between the liquid thin film with three droplets with diameter of $D = 37.4\ \mu m$ and five droplets with diameter of $D = 31.6\ \mu m$, giving the same total volume in all three cases. The kinetic energy of the droplets in those three case is constant, $E_k = 6.32\ 10^{-9}\ pJ$. But the total surface energy for each initial case is different, which are $E_S = 2.9 \cdot 10^{-10}\ pJ$,

$4.2 \cdot 10^{-10}$ *pJ* and $5.0 \cdot 10^{-10}$ *pJ* for Figure 1(A), (B) and (C), respectively.

Evidently, the effect of the shape of initial droplets is strong. Figure 1(B) demonstrates that three smaller satellite droplets come closer to penetrating than in the case of one single bigger droplet (see Figure 1(A)), but it is still not sufficient. The energy of droplets almost is lost. They are trapped in the thin liquid film, which went back to the original form after long simulation.

The introduction of five satellite droplets as shown in Figure 1(C) not only increases the total energy of the system but also extends the impact time of droplets to the liquid thin film. Consequently, it gives more time for the thin film to develop and have a secondary droplet is released from the thin film.

Figure 2 shows a sequence of pictures for the case shown in Figure 1(C). In Figure 2(B), the first two droplets have already touched the thin film. However, the energy of those two droplets is not sufficient to generate the second droplet behind the thin film until four droplets hit to the film as shown in Figure 2(C). The energy transferred to the thin film seems to be strong enough and the time is also long enough to generate the secondary droplet behind the thin film later as shown in Figure 2(D). It snaps the thin film and continues flying with its remaining momentum.

The whole sequence of Figure 2 shows an agreement with the experiment in which the liquid thin film functioned as a filter for satellite droplets, [1]. A change in the volume of droplets occurred in the numerical simulation and 60 *pl* remained after shot 80 *pl* through the thin liquid film.

Figure 3 shows the velocity profile at $t = 45.6$ μs. When droplets pass through the thin liquid film, a vortex around the secondary droplet is formed and forces this droplet to continue moving with the remaining velocity. Also there are several vortices around the thin film and those vortices force the thin film back to normal shape by surface tension force.

Recorded remaining speed, U_2, of droplets after passing through the thin film is found to strongly depend on the initial speed of droplets (dispensing velocity, U_0), Figure 4. As shown in this figure, the dependency of U_2 on U_0 is similar between numerical results and experimental results. In all the simulations shown in Figure 4, the liquid volume of the printhead was distributed in five equal droplets.

4 Conclusions

In this study, numerical simulation of micro two-phase flows with high density difference has been carried out. A diffuse interface formulation, namely, the Phase-Field method, is employed to capture the interface. The numerical results indicate that this method can successfully simulate the impact, mixing and pinch-off when a droplet is shot at a thin liquid film.

A series of simulations is performed that match the experimental conditions. The numerical result helps to understand the importance of the surface energy of the micro droplets when they impact with a thin liquid film. It also gives a detailed view of the generation of the secondary droplet behind the thin liquid film.

It was found that a sequence of five smaller droplets could easily penetrate the film, where a single larger droplet would not. This may seem surprising, since the total liquid volume and the initial speed, and thus the total momentum of the impact, was the same in both cases. However, when the volume is divided into a larger number of smaller droplets, the surface energy is partially converted to kinetic energy, and this helps the incident liquid to penetrate.

REFERENCES

[1] Geyl, A., Amberg, G., van der Wijngaart, W., and Stemme, G., 2006. "Study of the flight of small liquid droplets through a thin liquid film for picolitre liquid transfer". In proceeding of 19th IEEE International Conference on MEMS.

[2] Villanueva, W., and Amberg, G., 2006. "Some generic capillary-driven flows". *Int. J. of Multiphase Flow,* **32**, pp. 1072–1086.

[3] Jacqmin, D., 1999. "Calculation of two-phase Navier-Stokes flows using phase-field modeling". *J. Computational Physics,* **155**, pp. 96–127.

[4] Amberg, G., Tönhardt, R., and Winkler, C., 1999. "Finite element simulations using symbolic computing". *Mathematics and Computers in Simulation,* **49**, pp. 149–165.

[5] Davis, T., 2004. "Algorithm 832: Umfpack, an unsymmetric-pattern multifrontal method". *ACM Transactions on Mathematical Software,* **30**(2), pp. 196–199.

[6] Do-Quang, M., Villanueva, W., Singer-Loginova, I., and Amberg, G., 2007. "Parallel adaptive computation of some time-dependent materials-related microstructural problems". *Bulletin of the Polish academy of sciences,* **55**(2), p. 229.

[7] Guermond, J.-L., and Quartapelle, L., 2000. "A projection fem for variable density incompressible flows". *J. Comput. Phys.,* **165**(1), pp. 167–188.